Near-infrared [Fe II] emission from supernova remnants and the supernova rate of starburst galaxies

T. Morel,[1,2,3]★ R. Doyon[3] and N. St-Louis[3]

[1]*Inter-University Centre for Astronomy and Astrophysics (IUCAA), Post Bag 4, Ganeshkhind, Pune, 411 007, India*
[2]*Astrophysics Group, Imperial College of Science, Technology and Medicine, Blackett Laboratory, Prince Consort Road, London SW7 2BZ*
[3]*Département de Physique and Observatoire du Mont Mégantic, Université de Montréal, C. P. 6128, Succ. Centre-Ville, Montréal, Québec H3C 3J7, Canada*

ABSTRACT

In an effort better to calibrate the supernova rate of starburst galaxies as determined from near-infrared [Fe II] features, we report on a [Fe II] $\lambda 1.644 \, \mu$m line-imaging survey of a sample of 42 optically selected supernova remnants (SNRs) in M33. A wide range of [Fe II] luminosities are observed within our sample (from less than 6 to 695 $L_\odot$). Our data suggest that the bright [Fe II] SNRs are entering the radiative phase and that the density of the local interstellar medium (ISM) largely controls the amount of [Fe II] emission. We derive the following relation between the [Fe II] $\lambda 1.644 \, \mu$m line luminosity of *radiative* SNRs and the electronic density of the post-shock gas, n_e: $L_{[Fe\,II]}$ ($L_\odot$) $\approx 1.1 n_e$ (cm^{-3}). We also find a correlation in our data between $L_{[Fe\,II]}$ and the metallicity of the shock-heated gas, but the physical interpretation of this result remains inconclusive, as our data also show a correlation between the metallicity and n_e. The dramatically higher level of [Fe II] emission from SNRs in the central regions of starburst galaxies is most likely due to their dense environments, although metallicity effects might also be important. The typical [Fe II]-emitting lifetime of a SNR in the central regions of starburst galaxies is found to be of the order of 10^4 yr. On the basis of these results, we provide a new empirical relation allowing the determination of the current supernova rate of starburst galaxies from their integrated near-infrared [Fe II] luminosity.

Key words: surveys – supernova remnants – galaxies: individual: M33 – galaxies: starburst – infrared: ISM.

1 INTRODUCTION

Early near-infrared (near-IR) spectroscopic observations of galactic SNRs have shown that these objects present remarkably strong [Fe II] features (e.g. Graham, Wright & Longmore 1987). This has been proposed to be mainly due to the existence of an extended post-shock region in which the ionization conditions are such that Fe$^+$ can be efficiently excited by electron collisions (Mouri, Kawara & Taniguchi 2000). In contrast, the spatial extent of this zone, where hydrogen is partially ionized, is small in photoionized regions, resulting in little emission (e.g. Luhman, Engelbracht & Luhman 1998).

This peculiarity can be used as a diagnostic probe of supernova activity in distant starburst galaxies where the SNRs are generally unresolved and are thought to produce much of the integrated near-IR [Fe II] emission (e.g. Vanzi & Rieke 1997). Of particular interest is the fact that using near-IR [Fe II] lines to estimate supernova

activity can potentially be superior to the usual radio technique, in that it more clearly distinguishes H II regions from SNRs.

From estimates of the *total* [Fe II] luminosity of a starburst galaxy ($\mathcal{L}_{[Fe\,II]}$) and assumptions regarding the typical values of the [Fe II] luminosity ($L_{[Fe\,II]}$) and [Fe II]-emitting lifetime ($t_{[Fe\,II]}$) of a *single* SNR, one can define the supernova rate, η, as:

$$\eta = \frac{\mathcal{L}_{[Fe\,II]}}{t_{[Fe\,II]} \; L_{[Fe\,II]}} \; \text{yr}^{-1} \tag{1}$$

This quantity can be used, for instance, to set constraints on the star formation history of starburst galaxies (e.g. Leitherer & Heckman 1995; Kotilainen et al. 1996).

Unfortunately, the supernova rate derived by this technique is considerably uncertain, as it scales with $t_{[Fe\,II]}$ and $L_{[Fe\,II]}$ which are poorly known. The [Fe II]-emitting lifetime of a SNR is generally taken to be of the order of $1-2 \times 10^4$ yr, but this estimate lies on weak grounds (e.g. van der Werf et al. 1993). On the other hand, the few [Fe II] $\lambda 1.644 \, \mu$m luminosities quoted in the literature for SNRs in our Galaxy, the LMC or M33 span a wide range of values

★E-mail: morel@iucaa.ernet.in

(from 0.3 to 720 L$_\odot$; Graham et al. 1987; Oliva, Moorwood & Danziger 1989, 1990; Lumsden & Puxley 1995 – hereafter LP). One issue of particular importance is understanding why SNRs in starburst galaxies exhibit dramatically higher [Fe II] luminosities (up to 1.6×10^5 L$_\odot$ in M82; Greenhouse et al. 1997). Much higher values are also observed in NGC 253 (Forbes et al. 1993). Before using near-IR [Fe II] features to estimate supernova activity in star-forming galaxies that presumably exhibit widely different properties (e.g. metallicity), one must first understand what parameters control the [Fe II] properties of individual SNRs. Many factors (e.g. evolutionary status of the SNR, density or metallicity of the local interstellar medium, hereafter ISM) are susceptible to playing a role in producing this observed luminosity range, although their relative importance has yet to be established.

2 A NEAR-IR [Fe II] LINE-IMAGING SURVEY OF EXTRAGALACTIC SNRS

In an effort to address this issue, we present the results of a project in which narrow band images are used to secure [Fe II] $\lambda 1.644\,\mu$m luminosities for a large sample of extragalactic SNRs spanning a wide range of physical properties and evolutionary status. Previous efforts to determine the [Fe II] luminosities of individual SNRs have mainly concentrated on aperture photometry of galactic remnants. The shortcomings of such an approach are numerous: (i) those observations sample, in most cases, only a very small part of the SNR, rendering the total value of the [Fe II] luminosity considerably uncertain; (ii) because of the different apertures used, the published [Fe II] line luminosities do not constitute a homogeneous database based on which meaningful statistical studies can be conducted; (iii) the [Fe II] luminosities are uncertain, as the distance to these SNRs and the extinction corrections are generally poorly known. On the other hand, because of the unavoidable limited size of the aperture, surveys in nearby galaxies carried out using long-slit spectroscopy exclude the largest objects and are therefore biased towards the youngest SNRs (see LP). Line-imaging observations of SNR populations in local group galaxies do not suffer from these limitations.

M33 is an obvious target in this respect because of its relatively face-on orientation ($i \approx 55°$; Garcia-Gomez & Athanassoula 1991), well-known distance ($D \approx 840$ kpc; Freedman, Wilson & Madore 1991) and substantial abundance gradient that allows an investigation of metallicity effects (Smith et al. 1993). Furthermore, it has the largest catalogued extragalactic SNR population (Gordon et al. 1999). Of particular importance is the fact that a large body of observational data exists for SNRs in this galaxy; as will be shown below, this will allow us to relate the near-IR [Fe II] emission to observations in other parts of the electromagnetic spectrum. The latest catalogue of optically selected SNR candidates in M33 comprises 98 objects (Gordon et al. 1998), many of which are detected at radio frequencies (Gordon et al. 1999, and references therein). Among this sample, 72 objects have been spectroscopically confirmed and therefore also have well-defined optical-line properties (Gordon et al. 1998, and references therein). In addition, a *ROSAT* survey of M33 has associated some X-ray sources with known SNRs (Long et al. 1996).

3 OBSERVATIONS AND REDUCTION PROCEDURE

Our observations were obtained at the Canada–France–Hawaii Telescope (CFHT) in 1997 and 1998, using the IR cameras MONICA and REDEYE, respectively. For both observing runs, the cameras were equipped with a 256×256 pixels HgCdTe NICMOS-3 detector array. At the f/8 Cassegrain focus of the CFHT, the image scales are 0.246 (MONICA) and 0.5 arcsec pixel^{-1} (REDEYE). For the assumed distance to M33 ($D \approx 840$ kpc), this translates into a physical scale of 1 and 2 pc pixel^{-1}, respectively. In this configuration, the fields of view are about 63 (MONICA) and 128 arcsec (REDEYE). The interference filters used are a narrow-band filter (full width at half maximum, FWHM, $\approx 0.02\,\mu$m) centred on [Fe II] $\lambda 1.644\,\mu$m ($a^4D_{7/2} \rightarrow a^4F_{9/2}$) and a wide band H filter. The [Fe II] filter is sufficiently wide that the broadening due to motions of the remnant gas, the rotation or the redshift of M33 do not shift lines to significantly different parts of the transmission curve. In total, 42 objects drawn from the optically selected catalogue of Gordon et al. (1998) have been observed. The vast majority has been spectro-scopically confirmed (Blair & Kirshner 1985; Smith et al. 1993; Gordon et al. 1998). Particular attention has been paid to observe SNRs with widely different properties. The journal of observations is presented in Table 1.

For each SNR we have obtained five images: one centred on the object and four offset to the NW, NE, SW and SE by 22 and 45 arcsec for MONICA and REDEYE, respectively. These images were later combined in a mosaic centred on the SNR. Two type of dome flats have been obtained (dome lights 'on' and 'off'). The latter has been subtracted from the former in order to remove the contribution from the thermal background. These dome flats have been used to correct for changes in the quantum efficiency of the pixels in each object image. A mean sky frame has been created by applying a pixel-to-pixel median filtering procedure with proper masking of sources to the data frames themselves. No off-source images have been obtained. This procedure is justified in our case, as we are not attempting to detect uniform large-scale emission, but rather compact sources on the arcsecond scale (see Fig. 1). After subtraction of this mean sky frame to the individual object frames and multiplication by a bad pixel mask in order to account for dead pixels, the object images were aligned and coadded. The astrometric calibration was carried out with reference to positions of stars in the USNO-A2.0 or GSC1.2 catalogues. The positions are accurate to within 3 arcsec.

4 OVERVIEW OF THE SURVEY

Among our sample of 42 objects, only seven have been firmly detected (we address in Section 6.1 the physical reasons for such a low detection rate). Fig. 1 shows the [Fe II] and H-band images of this subset. The [Fe II] $\lambda 1.644\,\mu$m luminosities are quoted in Table 2, along with the 3σ upper limits for the remaining SNRs (column 14). The targets were observed at similar air masses as the standard stars, eliminating the need to correct for atmospheric extinction. This is legitimate in the H band, where such corrections are small. Using the optical extinction measurements of Blair & Kirshner (1985) and the interstellar reddening law of Rieke & Lebofsky (1985), it is also found that reddening corrections are negligible. The contribution of Br12 $\lambda 1.641\,\mu$m and [Si I] $\lambda 1.645\,\mu$m to the total flux in the [Fe II] filter has been neglected (see Oliva et al. 1989). The non-detection of any significant flux in the H-band images also indicates that the contribution from continuum emission is negligible (see also LP). The flux calibration was achieved by using faint standard stars in the list of Hunt et al. (1998). The internal accuracy is typically 0.011 mag in the H band. Some of our objects have been observed in near-IR spectroscopy

by LP. We have adopted their values whenever appropriate (i.e. when the object was detected in their survey but not in ours or when they set a more stringent upper limit). Four objects have been detected in both surveys and can be used to assess the robustness of our luminosity calibration (this is in particular necessary when considering that some of our observations were acquired while some cirrus clouds were present; see Table 1). In all cases, both values are found to agree within the uncertainties. The internal consistency of our data can also be examined by comparing repeated observations of SNR28 taken under different photometric conditions, as detailed in Table 1. Once again, these quantities are found to be statistically undistinguishable. These checks confirm the reliability of our derived luminosities.

The contour maps of the detected SNRs are shown in Fig. 2. Although the limited spatial resolution of our images prevents us to examine this aspect in detail, a comparison to *Hubble Space Telescope* (*HST*) or ground-based optical images (Blair & Davidsen 1993; Gordon et al. 1998) reveals roughly similar [Fe II]- and optical-line morphologies. We note significant differences between the diameters determined from our [Fe II] images and from optical observations (Gordon et al. 1998). This might result from difficulties in subjectively assigning diameters for objects with complex morphologies (see Blair & Davidsen 1993).

5   CORRELATIONS BETWEEN THE [Fe II] EMISSION AND OTHER SNR PROPERTIES

In order to pin down the physical processes that are responsible for the [Fe II] emission, we sought for correlations between the [Fe II] luminosities and various quantities intrinsic to the SNRs (e.g. optical-line properties). These data were gathered from the literature and are quoted in Table 2.

A number of statistical methods have been developed to investigate relationships between astronomical data sets with censored data (e.g. with upper limits). We made use here of the generalized Kendall's τ correlation technique (Isobe, Feigelson & Nelson 1986). Table 3 summarizes the results of this statistical analysis for all quantities under consideration. When a significant correlation is present (we consider this to be the case when the false alarm probability is less than 1 per cent), we give the results of a linear regression fit to the data for the *detected* objects (such regression techniques for censored data yield unreliable results in the presence of heavy censoring). We also show in Fig. 3 the dependence of $L_{[Fe II]}$ on the quantity in question. Survival analysis techniques yield more reliable results when the censored points are randomly distributed, a condition that is generally not fulfilled here (see Fig. 3). In order to assess the robustness of our results, we performed the same analysis when only considering firm detections. This procedure broadly confirms the correlations previously found (albeit with a lower level of significance), and suggests that the results inferred by taking into account all the available information (i.e. detections *and* upper limits) can be regarded as robust. We discuss below the implications of this statistical analysis on our understanding of [Fe II] emission in SNRs.

5.1   Optical-line properties

A significant correlation is found between all optical-line luminosities and $L_{[Fe II]}$ (Table 3). A good correlation between the [Fe II] and Hβ surface brightnesses has already been reported

for a sample of LMC and Galactic SNRs by Oliva et al. (1989). Although the optical and [Fe II] line-emitting regions are likely to differ in detail, this correlation suggests that the sites of [Fe II] emission are bright optical filaments whose emission is excited by radiative shocks. Support for this interpretation comes from observations of RCW 103 and N49 which show the [Fe II]- and optical-line morphologies to be virtually identical (Burton & Spyromilio 1993; Dickel et al. 1995). In both cases, the optical line-emitting regions are believed to trace the interaction of a radiative blast wave with a neighbouring molecular cloud (e.g. Banas et al. 1997; Oliva et al. 1999).

5.2   Density effects

A correlation is also found between the electronic density of the post-shock gas (as derived from the optical [S II] doublet) and $L_{[Fe II]}$. Near-IR [Fe II] features in SNRs are collisionally excited via electron impact in the dense recombination zone behind the shock front. The critical electron number density of [Fe II] $\lambda 1.644\,\mu$m is (Blietz et al. 1994):

$$n_c(T_4) \approx 4.2 \times 10^4 T_4^{0.69}\,\text{cm}^{-3} \qquad (2)$$

In this expression, T_4 is the electronic temperature in units of 10^4 K. For temperatures typical of [Fe II] line-emitting regions in SNRs ($T_e \approx 6500$ K; Oliva et al. 1989), collisional de-excitation becomes important for $n_e \approx 3.1 \times 10^4$ cm^{-3}. The post-shock densities are of the order of 10^3 cm^{-3} for the [Fe II] brightest remnants (Fig. 3b). However, the densities derived from the optical [S II] doublet have been generally found to be systematically lower (by about a factor of 5) than those determined from the near-IR [Fe II] lines, suggesting that the [Fe II] features are produced further downstream behind the shock (e.g. Oliva et al. 1989). The electronic densities prevailing in the [Fe II]-line emitting regions of the SNRs in our sample are thus less than 5×10^3 cm^{-3}, but are still much below the critical density for collisional de-excitation. In a two-level approximation, the luminosity of the [Fe II] $\lambda 1.644\,\mu$m transition is given by (Blietz et al. 1994):

$$L_{[Fe II]} = \pi^2 \frac{T_4^{-0.94}\,e^{-1.57/T_4}\,\mathcal{N}_{Fe^+}}{1 + n_c(T_4)/n_e} \left(\frac{d}{\text{cm}}\right)^2 \text{erg s}^{-1} \qquad (3)$$

Here $\mathcal{N}_{Fe^+}$ is the column density of Fe$^+$ in units of 10^{16} cm^{-2}, n_c is the critical density given by equation (2) and d is the diameter of the SNR. In view of the similar size of the detected SNRs (see Fig. 2), we will ignore in the following any dependence of $L_{[Fe II]}$ on the latter quantity. While $L_{[Fe II]}$ is only weakly dependent on the temperature (it varies within a factor of only 1.5 over five decades in density between 6000 and 20 000 K), it can be expressed to a reasonable degree of accuracy as a linear function of n_e for densities up to 10^4 cm^{-3}. The relationship found in our data between $L_{[Fe II]}$ and n_e ($L_{[Fe II]} \propto n_e^{1.244 \pm 0.188}$) is close to what might be expected from theoretical considerations. We will return to this point in the following.

The post-shock densities derived for the detected SNRs are 2 to 4 orders of magnitude higher than canonical values for the ISM ($n_0 \approx 0.1 - 10$ cm^{-3}). We have previously argued that the [Fe II] brightest SNRs are in the radiative expansion phase. Large compression factors (i.e. ratio of post-shock to pre-shock density) can be achieved for strong radiative shocks, with values in the range $10 - 50$ being typical (e.g. Vancura et al. 1992). While we cannot rule out the possibility that the high post-shock densities inferred for the detected SNRs are due to very large compression

Table 1. Journal of observations.

M33:SNR. ID[a] (1)	Other identifications[b] (2)	Coordinates (J2000)[c]		Exposure time (s)/Seeing (arcsec)		Date of observation (7)	Weather conditions (8)
		RA (3)	DEC (4)	[Fe II] $\lambda 1.644\,\mu m$ (5)	H (6)		
9	DDB-2, 013008 + 30241, V-13, D93-4, D95-3, G99-11	01 32 57.0	+ 30 39 26.2	3000/0.6	300/0.6	09/18/97	Clear
10	None	01 32 59.7	+ 30 30 41.3	2940/0.8	140/0.8	08/31/98	Clear
12	None	01 33 00.4	+ 30 31 00.3	2940/0.8	140/0.8	08/31/98	Clear
13	None	01 33 01.5	+ 30 30 45.2	2940/0.8	140/0.8	08/31/98	Clear
14	G99-17	01 33 03.5	+ 30 31 21.2	2940/0.8	140/0.8	08/31/98	Clear
15	SB-1, DDB-4, 013015 + 30245, V-17, D93-5, D95-4, G99-20	01 33 04.0	+ 30 39 53.5	2400/0.8	300/0.8	09/18/97	Clear
				1080/1.4	120/1.4	09/01/98	Clear
16	None	01 33 07.5	+ 30 42 51.8	2700/0.8	140/0.8	08/31/98	Clear
17	013021 + 30241, D93-6, D95-5, G99-24	01 33 10.0	+ 30 39 31.2	2700/1.4	240/1.4	09/01/98	Clear
18	013021 + 30270, D93-7	01 33 10.3	+ 30 42 22.3	2700/0.8	140/0.8	08/31/98	Clear
20	L96-11, 013022 + 30244, D93-9, D95-7, G99-25	01 33 11.2	+ 30 39 42.0	2700/1.4	240/1.4	09/01/98	Clear
21	NGC592, X-3, L96-12, G99-29	01 33 11.7	+ 30 38 40.0	1620/1.4	120/1.4	09/01/98	Clear
22	G99-35	01 33 17.3	+ 30 31 26.7	2700/0.8	100/0.8	08/31/98	Clear
23	None	01 33 21.5	+ 30 31 29.5	2700/0.8	100/0.8	08/31/98	Clear
24	G99-39	01 33 22.6	+ 30 27 03.6	2700/2.0	100/2.0	09/01/98	Clear, high humidity
25	DDB-5, G99-42	01 33 23.8	+ 30 26 11.6	2700/2.0	100/2.0	09/01/98	Clear, high humidity
26	G99-46	01 33 26.7	+ 30 47 47.9	2160/1.2	100/1.2	09/02/98	Clear
28	S-4, SB-5, DDB-6, 013040 + 30269, D93-10, D95-8, G99-50	01 33 29.0	+ 30 42 16.9	1500/0.6	300/0.6	09/17/97	A few cirrus clouds
				1920/0.7	200/0.7	08/30/98	Clear
29	L96-19, G99-52	01 33 29.6	+ 30 49 08.3	1080/1.2	40/1.2	09/02/98	Clear
30	G99-54	01 33 30.1	+ 30 47 44.8	2160/1.2	100/1.2	09/02/98	Clear
31	X-14, L96-20, DBS-1, S-5, DDB-7, 013042 + 30182, G-1, V-37, D93-11, D95-9, G99-57	01 33 31.3	+ 30 33 33.4	1500/0.6	300/0.6	09/17/97	A few cirrus clouds
32	L96-18, 013042 + 30269, D93-12	01 33 31.4	+ 30 42 19.3	600/0.6	120/0.6	09/17/97	A few cirrus clouds
				960/0.7	200/0.7	08/30/98	Clear
34	None	01 33 35.6	+ 30 49 22.7	540/1.2	20/1.2	09/02/98	Clear
35	L96-22, DBS-2, S-8, DDB-8, 013047 + 30211, G-2, V-44, D93-13, D95-10, G99-64	01 33 35.9	+ 30 36 27.3	1500/0.6	40/0.6	09/17/97	A few cirrus clouds
38	013049 + 30270, D93-16	01 33 37.9	+ 30 42 18.9	2700/1.2	100/1.2	09/02/98	Clear
41	013052 + 30272, D93-17	01 33 40.7	+ 30 42 31.8	2700/1.2	100/1.2	09/02/98	Clear
43	G99-77	01 33 41.7	+ 30 21 01.8	2700/2.0	100/1.2	09/01/98 ([Fe II])-09/02/98 (H)	Clear, high humidity (09/01)
44	G99-76	01 33 42.8	+ 30 41 50.9	2700/1.2	100/1.2	09/02/98	Clear
45	G99-81	01 33 43.5	+ 30 41 04.7	540/1.2	20/1.2	09/02/98	Clear
50	013102 + 30285, D93-21, D95-13, G99-103	01 33 51.1	+ 30 43 55.0	2700/0.9	300/0.9	09/18/97	Clear
				4860/0.7	60/0.7	08/30/98	Clear
54	G99-111	01 33 54.5	+ 30 45 19.2	720/0.7	20/0.7	08/30/98	Clear
55	MR-13, X-13, L96-29, DBS-3, S-16, DDB-9, 013106 + 30178, G-3, V-69, D93-23, D95-15, G99-112	01 33 54.7	+ 30 33 11.2	1500/0.6	300/0.6	09/17/97	A few cirrus clouds
57	013108 + 30196, D93-24, D95-16, G99-114	01 33 57.0	+ 30 34 58.7	720/0.8	40/0.8	08/31/98	Clear
58	013109 + 30225, D93-26	01 33 58.0	+ 30 37 55.1	3000/0.9	300/0.9	09/18/97	Clear
60	013110 + 30210, D93-28	01 33 58.5	+ 30 36 24.1	3420/0.8	100/0.8	08/31/98	Clear
66	None	01 34 01.3	+ 30 35 20.5	720/0.8	40/0.8	08/31/98	Clear
73	L96-35, S-22, SB-11, DDB-11, 013121 + 30271, V-91, D93-33, D95-22, G99-148	01 34 10.6	+ 30 42 22.6	1500/0.6	300/0.6	09/18/97	Clear

Table 1 – *continued*

M33:SNR. ID[a] (1)	Other identifications[b] (2)	Coordinates (J2000)[c] RA (3)	DEC (4)	Exposure time (s)/Seeing (arcsec) [Fe II] λ1.644 μm (5)	H (6)	Date of observation (7)	Weather conditions (8)
74	013124+30198, D93-34	01 34 12.7	+30 35 12.3	540/1.2	20/0.8	08/31/98 (*H*)- 09/01/98 ([Fe II])	Clear
80	013125+30192, V-94, D93-36	01 34 14.2	+30 34 33.8	540/1.2	20/0.8	08/31/98 (*H*)- 09/01/98 ([Fe II])	Clear
82	013126+30176, D93-39, G99-154	01 34 15.5	+30 32 59.7	1080/1.2	40/0.8	08/31/98 (*H*)- 09/01/98 ([Fe II])	Clear
86	DDB-14, 013130+30184, V-101, D93-41	01 34 19.2	+30 33 44.9	2760/1.2	100/0.8	08/31/98 (*H*)- 09/01/98 ([Fe II])	Clear
87	DDB-15, 013131+30186, D93-42	01 34 19.8	+30 33 56.4	2760/1.2	100/0.8	08/31/98 (*H*)- 09/01/98 ([Fe II])	Clear
94	DDB-16, D93-48	01 34 33.0	+30 46 38.7	2700/1.2	100/1.2	09/02/98	Clear

[a]Identifications from Gordon et al. (1998).
[b]References for other identifications: X-ray: MR-x: Markert & Rallis (1983) – X-x: Trinchieri, Fabbiano & Peres (1988) – L96-x: Long et al. 1996). Optical: DBS-x: D'Odorico, Benvenuti & Sabbadin (1978) – S-x: Sabbadin (1979) – SB-x: Sabbadin & Bianchini (1979) – DDB-x: D'Odorico, Dopita & Benvenuti (1980) – 013.xxx + 30.xxx (Long et al. 1990). Radio: G-x: Goss et al. (1980) – V-x: Viallefond et al. (1986) – D93-x: Duric et al. (1993) – D95-x: Duric et al. (1995) – G99-x: Gordon et al. (1999).
[c]In units of hours, minutes and seconds (RA) and degrees, arcminutes and arcseconds (DEC).

factors, we rather favour the idea that they are evolving in an ambient medium of high density. The tendency for the objects with high radio fluxes to be strong [Fe II] emitters supports this picture (Table 3). Because thermal X-ray emission from the shock-heated gas (which should dominate X-ray excitation in our sample) scales with ambient density (e.g. Magnier et al. 1997), X-ray data can also be used to assess the relevance of this interpretation. However, we find no evidence in our data for a relationship between the X-ray and the [Fe II] luminosities. A better knowledge of the X-ray properties of SNRs in M33 might shed some new light on this issue.

5.3 Metallicity effects

Abundances derived from modelling the optical-line properties of SNRs reflect to a large extent the chemical composition of the swept-up interstellar material (e.g. Russell & Dopita 1990), and can be characterized by the 'metallicity index', A, defined as: $\log(A) = 0.8 + 1/3[\log(N/H) + \log(O/H) + \log(S/H)]$ (Dopita et al. 1984). We find a correlation between $L_{[Fe II]}$ and A which might indicate that [Fe II] emission is enhanced in regions characterized by high ISM chemical abundances. The column density of Fe$^+$, $\mathcal{N}_{Fe^+}$, in equation (3) can be rewritten as:

$$\mathcal{N}_{Fe^+} = f_1 \delta X_{Fe} \mathcal{N}_H \text{ cm}^{-2} \qquad (4)$$

where f_1 is the ionization fraction of Fe$^+$, δ is the gas phase iron abundance, X_{Fe} is the solar abundance of iron relative to hydrogen and $\mathcal{N}_H$ is the column density of neutral and singly ionized hydrogen. It can be seen that the correlation found in our data between $L_{[Fe II]}$ and A is consistent with theoretical predictions.

One major difficulty with this interpretation lies, however, in the existence of a positive correlation between n_e and A (see Table 3 and Fig. 4). While there is no evidence in our data for a negative correlation between n_e and galactocentric distance, this might suggest that both the metallicity (see Smith et al. 1993) and the density of the ISM increase when progressing towards the inner parts of M33. In view of this unexpected result, it is not clear whether the correlation between $L_{[Fe II]}$ and A is fundamental or is mainly a density effect. It is conceivable, however, that a spread in the metallicity of the ambient ISM among our sample of SNRs contributes to the large scatter observed in the $L_{[Fe II]}-n_e$ relation. Variations in the depletion factor might also be relevant in this respect, as both theory and observations suggest that the fraction of iron-bearing grains returned to the gas phase by shocks may significantly vary from one SNR to another (Jones, Tielens & Hollenbach 1996; Oliva et al. 1999). The positive correlation between $L_{[Fe II]}$ and the iron abundance hinted at by equation (4) should be kept in mind when comparing the [Fe II] properties of SNR populations in host galaxies with widely different metallicities.

6 DISCUSSION

6.1 Near-IR [Fe II] emission from SNRs

In the light of the results presented above, we conclude that strong near-IR [Fe II] emission in SNRs is subordinated to the existence of a radiative blast wave propagating through an ambient material of high density (other physical processes than shocks might account for [Fe II] emission in very young SNRs; Graham et al. 1990). This
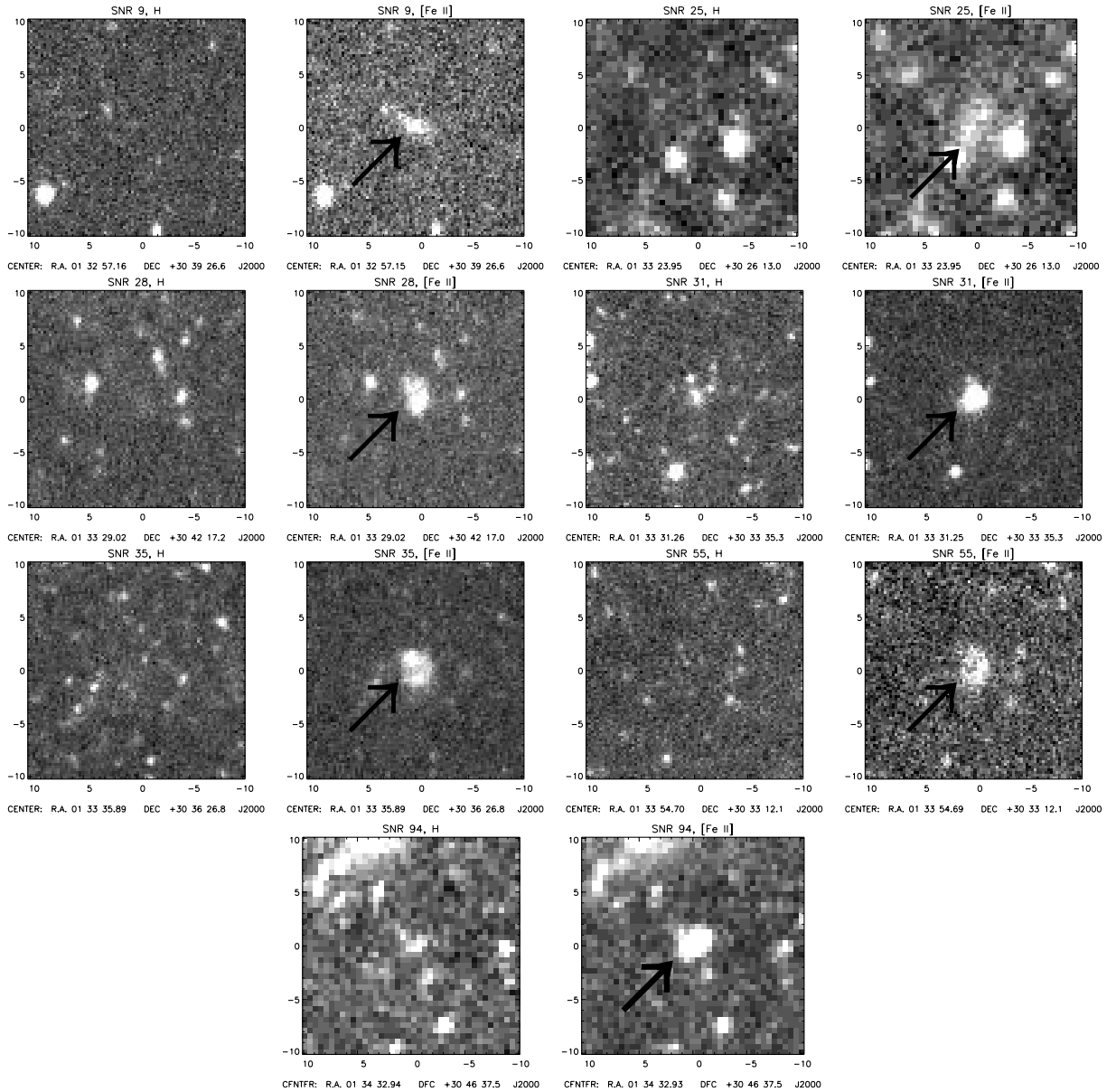
Figure 1. Comparison of the *H*-band (left-hand panels) and [Fe II] $\lambda 1.644\,\mu$m (right-hand panels) images of the detected SNRs. The identification of the SNR (taken from Gordon et al. 1998) is indicated on top of each panel. The location of the SNRs is indicated by an arrow. At the assumed distance to M33, 1 arcsec corresponds to 4.1 pc. The field of view is 20×20 arcsec. North is up and east is to the left.

picture is supported by the shock models of Hollenbach & McKee (1989). The [Fe II] brightest SNRs might be at the onset of the radiative phase, where line luminosities are believed to reach their maximum (Falle 1981; Cioffi & McKee 1988). We note that the relatively small size of our detected SNRs (Fig. 2) is not in conflict with the fact that they have reached such an advanced evolutionary stage; their confined nature may cause them to evolve rapidly. The low detection rate of our survey may result from: (i) the finite duration of strong [Fe II] emission in SNRs (see Section 6.4) and (ii) the fact that optically selected samples of SNRs are biased in favour of objects evolving in a tenuous medium, possibly the warm component of the ISM (e.g. Pannuti et al. 2000).

The following empirical relation has been found in our data between $L_{\rm [Fe\,II]}$ and $n_{\rm e}$ (see Table 3): $L_{\rm [Fe\,II]}$ (L$_\odot$) $\approx$ $0.257 n_{\rm e}^{1.244 \pm 0.188}$ (cm^{-3}). Because this exponent of 1.244 ± 0.188 is very close to the value of unity expected on theoretical grounds

(see Section 5.2), we shall consider in the following that

$$L_{\rm [Fe\,II]} = (1.1 \pm 0.3)\left(\frac{n_{\rm e}}{{\rm cm}^{-3}}\right) {\rm L}_\odot \qquad (5)$$

The factor 1.1 is simply the weighted average of $L_{\rm [Fe\,II]}/n_{\rm e}$. The equation above can be used to estimate the [Fe II] $\lambda 1.644\,\mu$m line luminosity of *radiative* SNRs from the sole knowledge of the electronic density in the post-shock region (as this relation refers to the density in the [S II]-emitting region, care should be taken when using other density diagnostics). We caution, however, that this relation has been derived on the basis of few detections that only sample a limited density regime. A better knowledge of the [Fe II] properties of SNRs in host galaxies with widely different ISM properties is needed to fully assess the

robustness of this relationship, especially with respect to metallicity effects.

6.2 Comparison with galactic and LMC SNRs

Is this picture consistent with [Fe II] observations of SNRs in our Galaxy and in the Large Magellanic Cloud (LMC)? These observations are summarized in Table 4, along with the typical post-shock densities associated with the SNRs considered. Great care has been taken to ensure that the density estimates (as determined from the [S II] doublet) relate to the same regions observed in [Fe II]. One major difficulty in comparing the [Fe II] luminosities of SNRs in M33 with their counterparts in our Galaxy or in the LMC lies in the extended nature of the latter class of objects. Most [Fe II] luminosities quoted in Table 4 are derived from aperture photometry and, in most cases, only sample a very small fraction of the SNR line-emitting regions. We performed an aperture correction to estimate the total [Fe II] luminosities by considering the ratio of the total optical size of the remnant to the area sustained by the aperture used.[1] We show in Fig. 5 the resulting [Fe II] luminosities of SNRs in M33, our Galaxy and the LMC, as a function of n_e. Although this investigation is not entirely conclusive owing to the crudeness of the corrections applied, interestingly it shows that the three objects in our sample of Galactic or LMC SNRs most unlikely to undergo radiative expansion (Crab, Kepler and N103B) fail by more than 2 orders of magnitude to follow the relationship between $L_{[Fe II]}$ and N_e. The Crab nebula and Kepler's remnant are both very young and therefore are still in the free (or Sedov–Taylor) expansion phase. The same is true for N103B which is likely to be still undergoing adiabatic expansion (Dickel & Milne 1995). The weakness of the [Fe II] emission in N103B and in Kepler's remnant illustrates the important point that the existence of radiative shocks is a necessary condition for strong [Fe II] emission, but *not* a high-density ambient ISM. As can be seen in Fig. 3(b), the [Fe II] luminosities of SNRs with similar densities may differ by as much as 2 orders of magnitude. This is best explained by evolutionary effects, with the low [Fe II] emitters being dominated by adiabatic shocks.

6.3 Implications for the [Fe II] emission of SNRs in starburst galaxies

The fact that the level of [Fe II] emission scales with density may help one to understand the differences that exist between the near-IR [Fe II] properties of SNR populations in galaxies with moderate star formation activity (such as M33) and starburst galaxies. While the present study demonstrates that the brightest remnants in M33 have [Fe II] luminosities of the order of $700 L_\odot$, SNRs in the starburst galaxy M82 have luminosities up to $1.6 \times 10^5 L_\odot$ (Greenhouse et al. 1997). Much higher values are also observed in NGC 253 (Forbes et al. 1993). We compare below the [Fe II] luminosities expected within the

framework of the results presented above with the observed values.

The electronic density in the [Fe II]-emitting regions of NGC 253 has been directly measured from density-sensitive near-IR [Fe II] line ratios and varies from $5 \times 10^3 \, \text{cm}^{-3}$ (Engelbracht et al. 1998) to $1 \times 10^4 \, \text{cm}^{-3}$ (Simpson et al. 1996). The [Fe II] emission in NGC 253 is believed to mainly arise from SNRs in the disk of the galaxy, and not from superwind- or AGN-related phenomena (Forbes et al. 1993). It is therefore reasonable to assume that these densities are typical of the post-shock regions of SNRs in the central regions of this galaxy. Keeping in mind that our empirical relation (equation 5) relates to the density derived from the [S II] doublet, and that the density in the [Fe II]-emitting region is about five times higher (e.g. Oliva et al. 1989), for these SNRs we estimate $L_{[Fe II]} \approx 1.1-2.2 \times 10^3 L_\odot$. This is in good agreement with the observed value, $L_{[Fe II]} \approx 2.6 \times 10^3 L_\odot$ (Forbes et al. 1993).

The ISM electronic densities prevailing in the central regions of M82 show a large spread: $n_0 = 50-500 \, \text{cm}^{-3}$ (Förster-Schreiber et al. 2001, and references therein). We shall consider in the following: $n_0 = 200 \, \text{cm}^{-3}$. This translates into: $n_e \approx 6 \times 10^3 \, \text{cm}^{-3}$, if one considers a canonical value for the compression factor of the SNR blast wave of 30. This estimate is consistent with the upper limit of $3.2 \times 10^4 \, \text{cm}^{-3}$ derived by Lester et al. (1990) from [Fe II] lines. According to equation (5), [Fe II] $\lambda 1.644 \, \mu m$ luminosities approaching $10^4 L_\odot$ can easily be reached for these SNRs. However, it appears that density effects alone have difficulties in explaining the high luminosities of the [Fe II] brightest sources in M82 (up to $1.6 \times 10^5 L_\odot$; Greenhouse et al. 1997). Two effects might account for this discrepancy. First, the SNR might expand in the interclump medium of molecular clouds, with the result that we severely underestimate n_e (Chevalier & Fransson 2001). Secondly, considering the high space density of SNRs in the compact star-forming regions of this galaxy (Huang et al. 1994), it is far from clear that the strong [Fe II] sources mapped by Greenhouse et al. (1997) can be identified with individual SNRs. The radius at which a SNR enters the radiative phase scales with the initial blast energy, E_{51}, and upstream hydrogen number density, n_H, as: $R_{rad} \propto E_{51}^{5/17} n_H^{-7/17}$ (Blondin et al. 1998). Regardless of the details of the original explosion, one therefore expects the bright [Fe II] SNRs in starburst galaxies to be less spatially extended (by a factor of 2–5) than the detected SNRs in M33 (with $\bar{d} \approx 21 \, \text{pc}$). It is thus plausible that the exceptionally strong [Fe II] sources in M82 (with sizes up to 40 pc) are made up of several individual SNRs with diameters in the range 4–10 pc.

We conclude that the dichotomy between the [Fe II] properties of SNRs in quiescent and in starburst galaxies may be interpreted as a result of the different ISM densities prevailing in both type of galaxies. Although clear metallicity effects have not been uncovered from our data, we also note that a substantial enrichment in metals is expected in the hostile environments of starburst regions (because of high chemical abundances and/or processing via grain destruction of the large reservoir of dust grains) and might also potentially contribute to strong [Fe II] emission.

6.4 The [Fe II]-emitting lifetime of SNRs

To estimate the typical [Fe II]-emitting lifetime of a SNR, we consider the integrated [Fe II] $\lambda 1.644 \, \mu m$ luminosity corrected for extinction in the central $2.4 \times 12 \, \text{arcsec}^2$ region of NGC 253 as

---

[1] We note that these corrections are likely to be grossly overestimated as the [Fe II] measurements are generally performed on the brightest optical knots where we expect the highest level of [Fe II] emission (see Section 5.1). For instance, we derive from the observations of Rho et al. (2001) a total dereddened [Fe II] $\lambda 1.644 \, \mu m$ luminosity for IC 443 of about $55 L_\odot$. This value is much smaller than our estimate of $1200 L_\odot$ derived from the measurements of Graham et al. (1987) through a 35×35 arcsec aperture.

Table 2. Properties of the sample.

M33:SNR.[a] ID (1)	d^b (pc) (2)	GCD^b (kpc) (3)	$\log(n_e)^b$ (cm^{-3}) (4)	$\log(A)^c$ (5)	v_{bulk}^d (km s^{-1}) (6)	L_X [0.1–2.4] keV^e (10^{36} erg s^{-1}) (7)	$\mathcal{F}$[O I] λ6300^f (8)	$\mathcal{F}$(Hα)^f (10^{-15} erg s^{-1} cm^{-2}) (9)	$\mathcal{F}$[N II] λ6584^f (10)	$\mathcal{F}$[S II] λ6717^f (11)	S_6^g (mJy) (12)	S_{20}^g (mJy) (13)	$L_{\text{[Fe II]}}^h$ (L$_\odot$) (14)
9	18	3.65	2.34	−3.78	263		2.01	11.5	2.50	4.65	0.4 ± 0.1	0.7 ± 0.2	59.9 ± 37.2
10	27	3.94											<203
12	26	3.84											<189
13	15	3.86											<61.0
14	27	3.64	<1.0				1.03	5.10	1.36	3.20	0.4 ± 0.1	1.1 ± 0.2	<300
15	48	3.25	<1.0	−4.12	183		3.17	20.3	4.53	6.36	0.4 ± 0.1	0.6 ± 0.1	37.3 ± 12.2^i
16	72	3.61											<1039
17	65	2.77	1.56	−3.87			<0.22	3.34	1.00	1.27	1.2 ± 0.2	2.3 ± 0.2	<651
18	15	3.37	<1.0	−3.67			0.73	2.91	0.80	1.61	<0.2	<0.2	<53.8
20	10	2.72	2.36	−3.72		1.94 ± 0.41	1.22	5.86	1.58	2.38	0.4 ± 0.1	0.8 ± 0.2	<5.67^i
21	28	2.57	2.43			28.5 ± 1.2	0.95	15.0	2.88	3.80	0.4 ± 0.1	0.9 ± 0.2	<174
22	37	3.19	<1.0				0.32	1.70	0.62	0.92	<0.3	0.3 ± 0.1	<335
23	68	3.14											<1142
24	22	4.67	<1.0				0.84	4.10	1.22	2.38	1.0 ± 0.1	1.8 ± 0.2	<72.3
25	27	5.00	1.89	−3.55			2.70	9.47	3.69	5.68	0.5 ± 0.1	1.4 ± 0.2	70.6 ± 28.6
26	49	4.21	1.84				0.64	4.30	0.96	2.06	<0.4	0.7 ± 0.2	<374
28	11	2.12	2.39	−3.32	345		6.20	16.6	7.27	9.89	0.6 ± 0.1	0.8 ± 0.2	475 ± 105^i
29	20	4.60	2.03			3.92 ± 0.53	0.25	1.60	0.46	0.67	0.2 ± 0.1	0.5 ± 0.1	<94.1
30	29	3.97	<1.0				<0.20	4.30	0.86	1.27	0.2 ± 0.1	0.4 ± 0.2	<163
31	39	2.28	2.90	−3.30	331	6.04 ± 0.64	16.3	72.9	43.6	30.6	0.7 ± 0.1	1.8 ± 0.1	671 ± 208
32	52	2.00	<1.0	−3.99		6.23 ± 0.64	<0.43	2.77	0.60	1.11	<0.3	<0.4	<836
34	26	4.41											<207
35	32	1.27	2.41	−3.43	313	2.26 ± 0.64	11.2	70.7	33.9	36.7	1.5 ± 0.1	3.5 ± 0.2	695 ± 217
38	20	1.62	1.38	−3.87			0.61	6.63	2.05	2.54	<0.2	<0.2	<85.8
41	99	1.55	<1.0	−3.90			0.93	19.4	6.47	7.00	<0.4	<0.5	<2349
43	34	7.25	<1.0				0.70	20.5	3.50	5.38	0.5 ± 0.2	1.3 ± 0.3	<192
44	25	1.24									<0.6	<0.9	<142
45	20	0.90	<1.0				0.68	4.20	1.75	2.21	0.6 ± 0.1	1.2 ± 0.1	<116
50	42	1.69	<1.0	−3.88			0.65	10.1	3.51	3.77	0.4 ± 0.1	0.4 ± 0.1	<432
54	16	2.20	1.26				5.34	34.1	12.1	16.6	0.5 ± 0.1	1.3 ± 0.1	<92.2
55	18	2.75	2.37	−3.62	272	3.89 ± 0.57	2.40	14.5	5.23	6.39	1.8 ± 0.1	4.4 ± 0.2	280 ± 98
57	21	2.11	1.38				1.50	3.75	1.55	3.26	0.1 ± 0.1	0.4 ± 0.1	<225
58	17	1.05	1.85				1.70	5.04	3.02	3.95	<0.2	<0.2	13.0 ± 4.3^i
60	9	1.68	2.16				1.03	2.58	1.71	2.02	<0.1	<0.1	<19.5
66	43	2.17											<616
73	17	1.45	2.32	−3.57	185	2.73 ± 0.48	7.97	20.1	8.98	13.4	0.1 ± 0.1	0.5 ± 0.1	303 ± 93^i
74	51	2.82	<1.0	−4.17			<0.29	2.82	0.78	0.87	<0.3	<0.4	<1040
80	30	3.14	1.09				0.65	14.8	2.84	4.03	<0.2	<0.2	<306
82	26	3.76	<1.0	−3.81			0.14	1.30	0.42	0.58	0.3 ± 0.1	0.4 ± 0.1	<230

Table 2 – *continued*

M33:SNR.[a] ID (1)	d[b] (pc) (2)	GCD[b] (kpc) (3)	log(n_e)[b] (cm^{-3}) (4)	log(A)[c] (5)	v_{bulk}[d] (km s^{-1}) (6)	L_X [0.1–2.4] keV[e] (10^{36} erg s^{-1}) (7)	$\mathcal{F}$([O I] λ6300)[f] (8)	$\mathcal{F}$(Hα)[f] (10^{-15} erg s^{-1} cm^{-2}) (9)	$\mathcal{F}$([N II] λ6584)[f] (10)	$\mathcal{F}$([S II] λ6717)[f] (11)	S_6[g] (mJy) (12)	S_{20}[g] (mJy) (13)	$L_{[Fe II]}$[h] (L$_\odot$) (14)
86	34	3.68	1.09	−3.95			0.83	11.2	2.41	4.05	0.1 ± 0.1	0.2 ± 0.1	<244
87	22	3.65	<1.0	−3.85			2.32	18.8	4.67	8.16	<0.2	<0.2	<103
94	11	3.23	2.65	−3.77	224		2.50	15.1	3.23	4.81	<0.2	<0.1	189 ± 51

[a] Identifications from Gordon et al. (1998).

[b] Diameters, galactocentric distances and post-shock electronic densities from Gordon et al. (1998).

[c] 'Metallicity index' defined as log(A) = 0.8 + 1/3[log(N/H) + log(O/H) + log(S/H)] (see Dopita et al. 1984). From Blair & Kirshner (1985); Smith et al. (1993).

[d] Kinematic data from Blair, Chu & Kennicutt (1988).

[e] X-ray data from Long et al. (1996). A SNR is considered to be the counterpart of a X-ray source when both are spatially coincident to within 30 arcsec. As discussed by Long et al. (1996), hardness ratios support the associations.

[f] Optical spectrophotometric data from Blair & Kirshner (1985); Smith et al. (1993); Gordon et al. (1998). Except for SNR94, the optical fluxes are not dereddened. Note that these fluxes are derived from long-slit spectroscopy and are therefore likely to be slightly underestimated.

[g] Flux densities at 6 and 20 cm from Duric et al. (1993); Gordon et al. (1999).

[h] [Fe II] λ1.644 μm line luminosities (assuming isotropic emission and a distance to M33 of 840 kpc; Freedman et al. 1991), along with the 1σ uncertainties. The upper limits are quoted for a statistical significance of 3σ and assuming similar sizes for the [Fe II]- and [S II]-emitting regions. As a consequence, observations of SNRs with various sizes under identical weather conditions and integration times yield different upper limits.

[i] Derived from the [Fe II] λ1.257 μm fluxes of LP, assuming a distance of 840 kpc and the theoretical (i.e. uncorrected for extinction ratio: [Fe II] λ1.257 μm/[Fe II] λ1.644μm = 1.36 (Nussbaumer & Storey 1988). As discussed by LP, their photometry is subject to large systematic uncertainties. A typical value of 30 per cent has been considered in addition to the uncertainties quoted in their table 2.

[j] Unweighted mean of repeated observations.

$L_{[Fe II]} \approx 1.3 \times 10^5$ L$_\odot$ (Engelbracht et al. 1998). A distance of 2.5 Mpc has been adopted (De Vaucouleurs 1978). We have also assumed a homogeneous mixture of gas and dust with an extinction towards the [Fe II]-emitting regions of $A_V = 8.4$ mag (Engelbracht et al. 1998) and the interstellar extinction law of Rieke & Lebofsky (1985). The *global* radio supernova rate of NGC 253 is uncertain, but estimates range from 0.1 to 0.2 yr^{-1} (Ulvestad 2000, and references therein). A value $\eta \approx 0.15$ yr^{-1} is adopted in the following. To translate this into a normalized value for the central 2.4×12 arcsec^2 region, we consider the ratio of the area sustained by this aperture by the total radio extent of the galaxy, which gives: 9×10^{-3} yr^{-1}. The electron density in the [Fe II]-emitting regions lies in the range: $5–10 \times 10^3$ cm^{-3} (Simpson et al. 1996; Engelbracht et al. 1998). Using equation (5) by converting to densities in the [S II]-emitting regions, and substituting the result in equation (1) yields $t_{[Fe II]} \approx 0.7–1.4 \times 10^4$ yr.

Similar calculations can be applied to M82. The integrated [Fe II] λ1.644 μm luminosity corrected for extinction in the central 16×10 arcsec region is: $L_{[Fe II]} \approx 2.7 \times 10^6$ L$_\odot$ (Förster-Schreiber et al. 2001). A distance of 3.3 Mpc (Freedman & Madore 1988) and the similar extinction model as above, with $A_V = 36$ mag, has been adopted (Förster-Schreiber et al. 2001). By considering this relatively small area in M82, we minimize the contribution of large-scale, superwind-induced emission (Greenhouse et al. 1997). Radio observations yield a global supernova rate of $\eta = 0.11 \pm 0.05$ yr^{-1}, which translates into a normalized value for the central 16×10 arcsec region of about 0.016 yr^{-1} (Huang et al. 1994). Additionally, we assume the typical [Fe II] luminosity for SNRs in M82 as determined previously, $L_{[Fe II]} \approx 10^4$ L$_\odot$. Substituting in equation (1) yields $t_{[Fe II]} \approx 1.7 \times 10^4$ yr.

Considering the large uncertainties involved, the values of $t_{[Fe II]}$ for SNRs in NGC 253 and M82 appear to be in good agreement. The [Fe II]-emitting lifetime derived for NGC 253 is more robust, as the density of the [Fe II]-emitting gas has been directly measured in this galaxy. A value of 1×10^4 yr will thus be adopted in the following. This estimate is broadly consistent with the duration of strong optical emission in SNRs, as determined by evolutionary models (e.g. Franco et al. 1994).

6.5 The supernova rate of starburst galaxies

By using equation (5) and the [Fe II]-emitting lifetime derived above, the supernova rate given by equation (1) can be written as a function of the *post-shock* electron density as:

$$\eta \approx \frac{\mathcal{L}_{[Fe II]}/L_\odot}{1.1 \times 10^4} \left(\frac{n_e}{cm^{-3}} \right)^{-1} yr^{-1}. \tag{6}$$

In the absence of density diagnostics for the post-shock regions, this expression can be conveniently expressed as a function of the (more easily measurable) ISM number density, n_0, by an appropriate choice of the typical compression factor of the SNR blast wave.

Considering the various assumptions made here and the fact that metallicity issues still remain to be fully addressed, the supernova rate we derive is still uncertain. In spite of these limitations, we note that our expression is consistent with previous estimates (van der Werf et al. 1993; Vanzi & Rieke 1997) if canonical ISM densities for starburst galaxies are considered ($n_0 \approx 100$ cm^{-3}). The relation proposed by van der Werf et al. (1993) has been found to give a good agreement in a
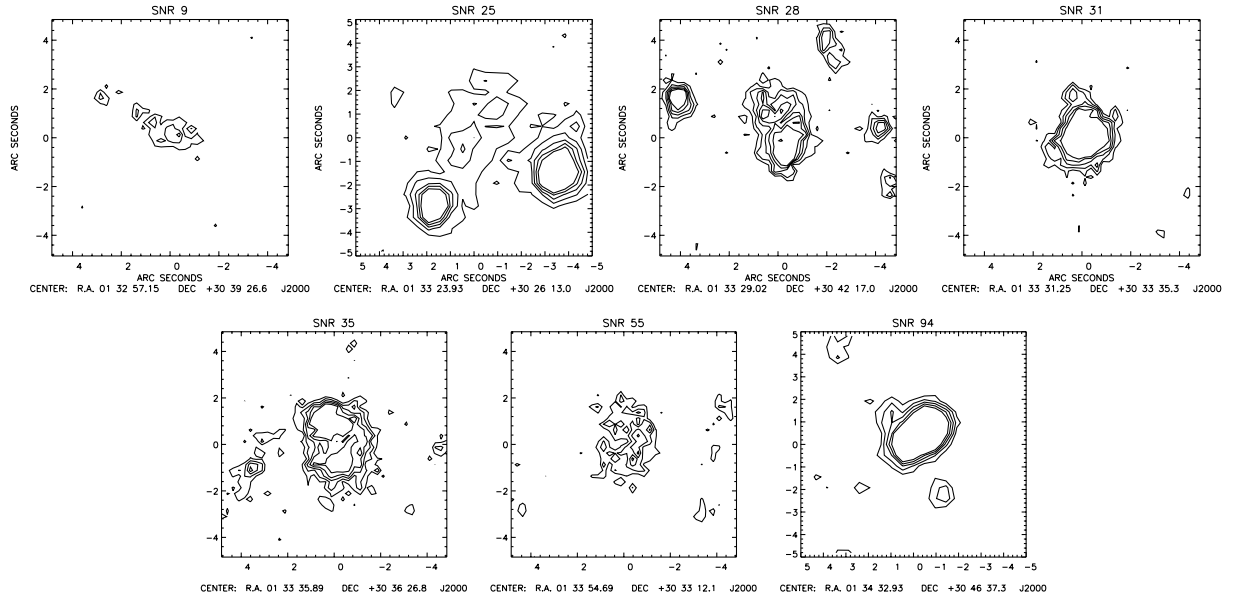
Figure 2. Contour maps of the detected SNRs. The identification of the SNR (taken from Gordon et al. 1998) is indicated on top of each panel. The contours are drawn from 3σ to 11σ, by steps of 2σ. At the assumed distance to M33, 1 arcsec corresponds to 4.1 pc. The field of view is 10×10 arcsec. North is up and east is to the left.

Table 3. Results of the statistical analysis. N: Number of points included in the calculations. $\mathcal{P}(X,Y)$: Probability for a chance correlation between the variables X and Y (data from Table 2). Note that the objects at large galactocentric distances, *GCD*, show a tendency for *lower* $L_{\text{[Fe II]}}$ and n_e values.

X	Y	N	$\mathcal{P}(X,Y)$ (per cent)	N	$\mathcal{P}(X,Y)$ (per cent) (detections only)	$\log X = (a \pm \sigma_a) \log Y + (b \pm \sigma_b)$ (detections only)
(1)	(2)	(3)	(4)	(5)	(6)	(7)
$L_{\text{[Fe II]}}$	Dynamical age[a]	42	82	10	100	
	$L([O\,\textsc{i}]\,\lambda6300)$	34	0.1	10	1.6	$\log(L_{\text{[Fe II]}}) = (1.345 \pm 0.167)\ \log(L[O\,\textsc{i}]\lambda6300) + (-0.402 \pm 0.343)$
	$L(H\alpha)$	34	0.2	10	2.5	$\log(L_{\text{[Fe II]}}) = (1.174 \pm 0.159)\ \log(LH\alpha) + (-0.771 \pm 0.422)$
	$L([N\,\textsc{ii}]\,\lambda6584)$	34	0.1	10	0.6	$\log(L_{\text{[Fe II]}}) = (0.949 \pm 0.133)\ \log(L[N\,\textsc{ii}]\lambda6584) + (0.210 \pm 0.300)$
	$L([S\,\textsc{ii}]\,\lambda6717)$	34	0.1	10	0.2	$\log(L_{\text{[Fe II]}}) = (1.244 \pm 0.165)\ \log(L[S\,\textsc{ii}]\lambda6717) + (-0.577 \pm 0.388)$
	v_{bulk}	8	8.3	8	8.3	
	n_e	34	0.1	9	3.7	$\log(L_{\text{[Fe II]}}) = (1.244 \pm 0.188)\ \log(n_e) + (-0.590 \pm 0.454)$
	S_6	35	1.5	8	11	
	S_{20}	35	2.2	8	14	
	A[b]	20	0.2	9	0.7	$\log(L_{\text{[Fe II]}}) = (1.380 \pm 0.216)\ \log(A) + (7.342 \pm 0.768)$
	L_X	8	53	4	50	
	GCD	42	8.5	10	18	
n_e	A[b]	20	0.1	12	1.1	$\log(n_e) = 1.753 \log(A) + 8.530$
	GCD	34	18	20	52	

[a]The dynamical ages have been derived using equation (5) of Gordon et al. (1998).
[b]'Metallicity index': see Section 5.3 for definition.
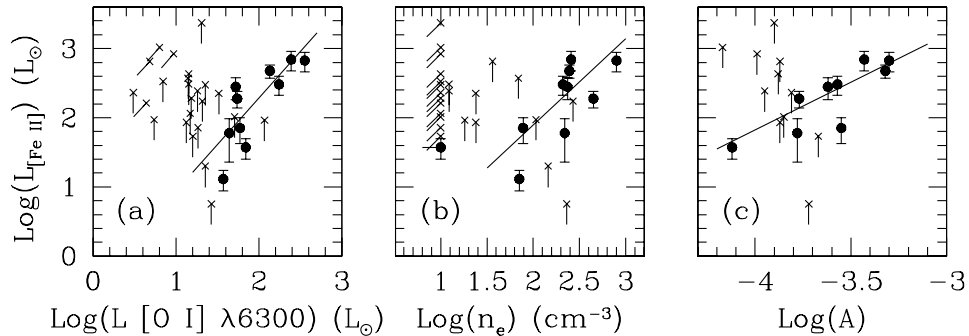
Figure 3. Variation of $L([Fe\,\textsc{ii}]\,\lambda1.644\,\mu\text{m})$ with (a) $L([O\,\textsc{i}]\,\lambda6300)$, (b) n_e and (c) the 'metallicity index' A (data from Table 2). These three quantities show a statistically significant correlation ($\mathcal{P} < 1$ per cent) with $L_{\text{[Fe II]}}$ (see Table 3). Filled circles are firm detections while the crosses denote 3σ upper limits. The solid line shows the results of a linear regression fit derived from χ^2 fitting of the data for the *detected* objects. Note that panel (a) is meant to illustrate the correlation between the optical- and [Fe II]-line luminosities. Similar variations are observed for the other optical transitions.
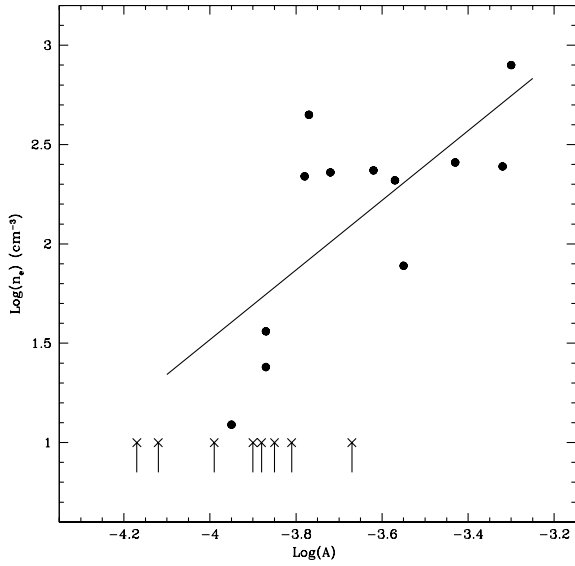
Figure 4. Variation of n_e with A. These two quantities show a statistically significant correlation (see Table 3). Filled circles are firm detections while the crosses denote 3σ upper limits. The solid line shows the results of a linear regression fit derived from χ^2 fitting of the points with a firm n_e determination.
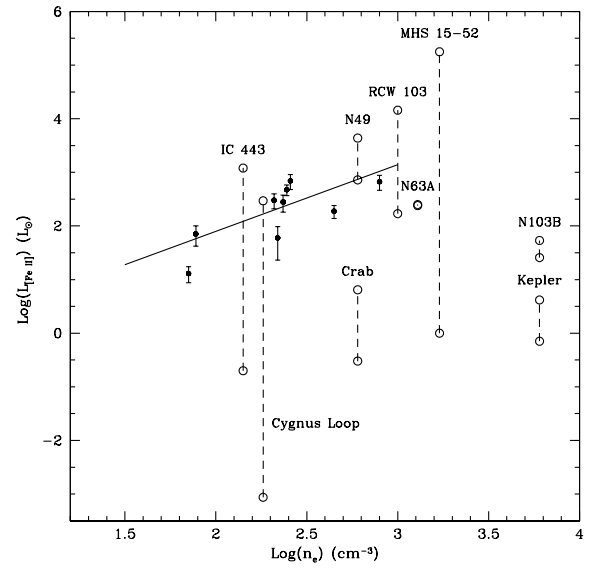
Figure 5. Variation of $L_{[Fe\,II]}$ with n_e for the detected SNRs in M33 (filled dots) and for a sample of SNRs in our Galaxy and in the LMC (open dots). The dashed lines illustrate the aperture corrections applied to the [Fe II] luminosities of the latter class of objects (see text). The solid line shows the results of a linear regression fit derived from χ^2 fitting of the SNRs in M33 with a firm n_e determination.

Table 4. $L_{[Fe\,II]}$ and post-shock electronic densities for LMC and Galactic SNRs.

Object	D (kpc)	Optical size (arcsec)	$L_{[Fe\,II]}^a$ ($L_\odot$)	Aperture size (arcsec)	Ref.	n_e([S II]) ($10^3\,cm^{-3}$)	Aperture^b ID	Ref.^{c}
(1)	(2)	(3)	(4)	(5)	(6)	(7)	(8)	(9)
N63A	52	25×25	240	20×30	1	1.3	–	2
N49	52	65×65	720	20×35	1	0.6	d and e	3
N103B	52	25×25	26	20×15	1	6.0	–	2
RCW 103	6.0	340×560	170^d	75×30	1	1.0	2	4
MHS 15–52	4.2	2100×2100^e	1.0	5×5	5	1.7	–	5
Kepler	4.0	21×64	0.7	15×15	1	6.0	1 and 2^f	4
Crab	2.0	290×420	0.3^g	75×75	1	0.6	3–8 and 10	6
IC 443	1.5	2700×2700^e	0.2^h	35×35	7	0.1	1–3	8
Cygnus Loop	0.44	$13\,800 \times 9600^e$	9×10^{-4}	20×20	9	0.2	1	10

^{a}[Fe II] $\lambda1.644\,\mu m$ luminosities corrected for extinction.
^{b}Apertures where the [S II] ratios have been determined. The mean of the [S II] ratios has been considered when several aperture IDs are given.
^{c}[S II] ratio from these references; the electronic densities have been derived using the diagnostic diagram (see their fig.6) of Blair & Kirshner (1985).
^{d}See also Oliva et al. (1999) for measurements through smaller apertures.
^{e}From Green (2000).
^{f}Corresponds to knot #27 of D'Odorico et al. (1986).
^{g}See also Graham et al. (1990), Hudgins, Herter & Joyce (1990) and Rudy, Rossano & Puetter (1994) for measurements of near-IR [Fe II] line fluxes through smaller apertures.
^{h}Because of the existence of noticeable density gradients across this SNR (and the related difficulty in assigning a typical density), the total value of Rho et al. (2001) is not considered here.
References – (1): Oliva et al. (1989); (2) Danziger & Leibowitz (1985); (3) Vancura et al. (1992); (4) Leibowitz & Danziger (1983); (5) Seward et al. (1983); (6) Fesen & Kirshner (1982); (7) Graham et al. (1987); (8) Fesen & Kirshner (1980); (9) Graham et al. (1991); (10) Miller (1974).

sample of starburst galaxies between supernova rates derived from near-IR [Fe II] lines and from their star-forming properties (Calzetti 1997). This provides some support to the validity of equation (6) to provide robust estimates of the supernova rates in galaxies with widely different ISM properties and for which the contribution of superwinds- and AGN-related phenomena to the total [Fe II] output can be neglected. Because only radiative

SNRs significantly contribute to $\mathcal{L}_{[Fe\,II]}$, however, these values are only lower limits.

7 CONCLUSIONS

The main conclusions of this study are the following:

(i) We have carried out the first near-IR [Fe II] line-imaging survey of extragalactic SNRs, presenting evidence for large intrinsic differences in their [Fe II] properties.

(ii) A significant correlation is found between the optical- and [Fe II]-line luminosities, suggesting that the detected SNRs are dominated by radiative shocks.

(iii) We suggest that the SNRs with strong [Fe II] emission are evolving in a dense ISM. Density effects are most probably the cause of the very strong level of [Fe II] emission from SNRs in starburst galaxies.

(iv) The typical [Fe II]-emitting lifetime of a SNR in starburst galaxies is found to be of the order of 10^4 yr.

(v) We provide a new empirical expression for the supernova rate of starburst galaxies, as derived from their integrated near-IR [Fe II] luminosity.

ACKNOWLEDGMENTS

REFERENCES

Banas K. R., Hughes J. P., Bronfman L., Nyman L.-Å., 1997, ApJ, 480, 607
Blair W. P., Chu Y.-H., Kennicutt R. C., 1988, in Roger R. S., Landecker T. L., eds, Proc. IAU Colloq. 101, Supernova Remnants and the Interstellar Medium. Cambridge Univ. Press, Cambridge, p. 193
Blair W. P., Kirshner R. P., 1985, ApJ, 289, 582
Blair W. P., Davidsen A. F., 1993, PASP, 105, 494
Blietz M., Cameron M., Drapatz S., Genzel R., Krabbe A., van der Werf P. P., Sternberg M., Ward M., 1994, ApJ, 421, 92
Blondin J. M., Wright E. B., Borkowski K. J., Reynolds S. P., 1998, ApJ, 500, 342
Burton M., Spyromilio J., 1993, Pub. Astron. Soc. Aus., 10, 327
Calzetti D., 1997, AJ, 113, 162
Chevalier R. A., Fransson C., 2001, ApJ, 558, L27
Cioffi D. F., McKee C. F., 1988, in Roger R. S., Landecker T. L., eds, Proc. IAU Colloq. 101, Supernova Remnants and the Interstellar Medium. Cambridge Univ. Press, Cambridge, p. 435
Danziger I. J., Leibowitz E. M., 1985, MNRAS, 216, 365
De Vaucouleurs G., 1978, ApJ, 224, 710
Dickel J. R., Milne D. K., 1995, AJ, 109, 200
Dickel J. R. et al., 1995, ApJ, 448, 623
D'Odorico S., Benvenuti P., Sabbadin F., 1978, A&A, 63, 63
D'Odorico S., Dopita M. A., Benvenuti P., 1980, A&AS, 40, 67
D'Odorico S., Bandiera R., Danziger I. J., Focardi P., 1986, AJ, 91, 1382
Dopita M. A., Binette L., D'Odorico S., Benvenuti P., 1984, ApJ, 276, 653
Duric N., Viallefond F., Goss W. M., van der Hulst J. M., 1993, A&AS, 99, 217
Duric N., Gordon S. M., Goss W. M., Viallefond F., Lacey C., 1995, ApJ, 445, 173

Engelbracht C. W., Rieke M. J., Rieke G. H., Kelly D. M., Achtermann J. M., 1998, ApJ, 505, 639
Falle S. A. E. G., 1981, MNRAS, 195, 1011
Fesen R. A., Kirshner R. P., 1980, ApJ, 242, 1023
Fesen R. A., Kirshner R. P., 1982, ApJ, 258, 1
Forbes D. A., Ward M. J., Rotaciuc V., Blietz M., Genzel R., Drapatz S., van der Werf P. P., Krabbe A., 1993, ApJ, 406, L11
Förster-Schreiber N. M., Genzel R., Lutz D., Kunze D., Sternberg A., 2001, ApJ, 552, 544
Franco J., Miller W. W., III, Arthur S. J., Tenorio-Tagle G., Terlevich R., 1994, ApJ, 435, 805
Freedman W. L., Madore B. F., 1988, ApJ, 332, L63
Freedman W. L., Wilson C. D., Madore B. F., 1991, ApJ, 372, 455
Garcia-Gomez C., Athanassoula E., 1991, A&AS, 89, 159
Gordon S. M., Kirshner R. P., Long K. S., Blair W. P., Duric N., Smith R. C., 1998, ApJS, 117, 89
Gordon S. M., Duric N., Kirshner R. P., Goss W. M., Viallefond F., 1999, ApJS, 120, 247
Goss W. M., Ekers R. D., Danziger I. J., Israel F. P., 1980, MNRAS, 193, 901
Graham J. R., Wright G. S., Longmore A. J., 1987, ApJ, 313, 847
Graham J. R., Wright G. S., Longmore A. J., 1990, ApJ, 352, 172
Graham J. R., Wright G. S., Hester J. J., Longmore A. J., 1991, AJ, 101, 175
Green D. A., 2000, A catalogue of Galactic Supernova Remnants (2000 August version). Mullard Radio Astronomy Observatory, Cavendish Laboratory, Cambridge, (available on the WWW at http://www.mrao.cam.ac.uk/surveys/snrs/)
Greenhouse M. A. et al., 1997, ApJ, 476, 105
Hollenbach D., McKee C. F., 1989, ApJ, 342, 306
Huang Z. P., Thuan T. X., Chevalier R. A., Condon J. J., Yin Q. F., 1994, ApJ, 424, 114
Hudgins D., Herter T., Joyce R. J., 1990, ApJ, 354, L57
Hunt L. K., Mannucci F., Testi L., Migliorini S., Stanga R. M., Baffa C., Lisi F., Vanzi L., 1998, AJ, 115, 2594
Isobe T., Feigelson E. D., Nelson P. I., 1986, ApJ, 306, 490
Jones A. P., Tielens A. G. G. M., Hollenbach D. J., 1996, ApJ, 469, 740
Kotilainen J. K., Forbes D. A., Moorwood A. F. M., van der Werf P. P., Ward M. J., 1996, A&A, 313, 771
Leibowitz E. M., Danziger I. J., 1983, MNRAS, 204, 273
Leitherer C., Heckman T. M., 1995, ApJS, 96, 9
Lester D. F., Carr J. S., Joy M., Gaffney N., 1990, ApJ, 352, 544
Long K. S., Blair W. P., Kirshner R. P., Winkler P. F., 1990, ApJS, 72, 61
Long K. S., Charles P. A., Blair W. P., Gordon S. M., 1996, ApJ, 466, 750
Luhman K. L., Engelbracht C. W., Luhman M. L., 1998, ApJ, 499, 799
Lumsden S. L., Puxley P. J., 1995, MNRAS, 276, 723, (LP)
Magnier E. A., Primini F. A., Prins S., van Paradijs J., Lewin W. H. G., 1997, ApJ, 490, 649
Markert T. H., Rallis A. D., 1983, ApJ, 275, 571
Miller J. S., 1974, ApJ, 189, 239
Mouri H., Kawara K., Taniguchi Y., 2000, ApJ, 528, 186
Nussbaumer H., Storey P. J., 1988, A&A, 193, 327
Oliva E., Moorwood A. F. M., Danziger I. J., 1989, A&A, 214, 307
Oliva E., Moorwood A. F. M., Danziger I. J., 1990, A&A, 240, 453
Oliva E., Lutz D., Drapatz S., Moorwood A. F. M., 1999, A&A, 341, L75
Pannuti T. G., Duric N., Lacey C. K., Goss W. M., Hoopes C. G., Walterbos R. A. M., Magnor M. A., 2000, ApJ, 544, 780
Rho J., Jarrett T. H., Cutri R. M., Reach W. T., 2001, ApJ, 547, 885
Rieke G. H., Lebofsky M. J., 1985, ApJ, 288, 618
Rudy R. J., Rossano G. S., Puetter R. C., 1994, ApJ, 426, 646
Russell S. C., Dopita M. A., 1990, ApJS, 74, 93
Sabbadin F., 1979, A&A, 80, 212
Sabbadin F., Bianchini A., 1979, PASP, 91, 62
Seward F. D., Harnden F. R., Murdin P., Jr, Clark D. H., 1983, ApJ, 267, 698
Simpson C., Forbes D. A., Baker A. C., Ward M. J., 1996, MNRAS, 283, 777
Smith R. C., Kirshner R. P., Blair W. P., Long K. S., Winkler P. F., 1993, ApJ, 407, 564
Trinchieri G., Fabbiano G., Peres G., 1988, ApJ, 325, 531

Ulvestad J. S., 2000, AJ, 120, 278

van der Werf P. P., Genzel R., Krabbe A., Blietz M., Lutz D., Drapatz S., Ward M. J., Forbes D. A., 1993, ApJ, 405, 522

Vancura O., Blair W. P., Long K. S., Raymond J. C., 1992, ApJ, 394, 158

Vanzi L., Rieke G. H., 1997, ApJ, 479, 694

Viallefond F., Goss W. M., van der Hulst J. M., Crane P. C., 1986, A&AS, 64, 237

This paper has been typeset from a TEX/LATEX file prepared by the author.